Polarization-Induced Local Pore-Wall Functionalization for Biosensing: From Micropore to Nanopore

ARTICLE *in* ANALYTICAL CHEMISTRY · FEBRUARY 2012

Impact Factor: 5.64 · DOI: 10.1021/ac2033744 · Source: PubMed

analytical chemistry

Article

pubs.acs.org/ac

Polarization-Induced Local Pore-Wall Functionalization for Biosensing: From Micropore to Nanopore

Jie Liu,*[,†] Pascale Pham,[‡] Vincent Haguet,[§] Fabien Sauter-Starace,[‡,∥] Loïc Leroy,[†] André Roget,[†] Emeline Descamps,[†] Aurélie Bouchet,[§] Arnaud Buhot,[†] Pascal Mailley,*[,†,⊥] and Thierry Livache[†]

[†]SPrAM, UMR5819, CEA/CNRS/UJF, INAC, [‡]CEA/LETI/DTBS, [§]Laboratoire BGE, U1038, CEA/Inserm/UJF, iRTSV, [∥]CEA/LETI/Clinatec, 17 rue des Martyrs, 38054 Grenoble Cedex 9, France

[⊥]LSE, INES-CEA 50 avenue du Lac Léman BP 332, 73377 Le Bourget du Lac cedex, France

Supporting Information

ABSTRACT: The use of biological-probe-modified solid-state pores in biosensing is currently hindered by difficulties in pore-wall functionalization. The surface to be functionalized is small and difficult to target and is usually chemically similar to the bulk membrane. Herein, we demonstrate the contactless electrofunctionalization (CLEF) approach and its mechanism. This technique enables the one-step local functionalization of the single pore wall fabricated in a silica-covered silicon membrane. CLEF is induced by polarization of the pore membrane in an electric field and requires a sandwich-like composition and a conducting or semiconducting core for the pore membrane. The defects in the silica layer of the micropore wall enable the creation of an electric pathway through the silica layer, which allows electrochemical reactions to take place locally on the pore wall. The pore diameter is not a limiting factor for local wall modification using CLEF. Nanopores with a diameter of 200 nm fabricated in a silicon membrane and covered with native silica layer have been successfully functionalized with this method, and localized pore-wall modification was obtained. Furthermore, through proof-of-concept experiments using ODN-modified nanopores, we show that functionalized nanopores are suitable for translocation-based biosensing.

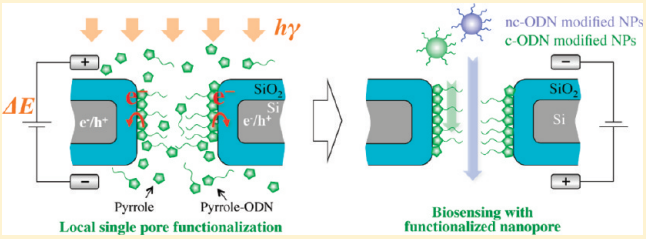

INTRODUCTION

The translocation of biological species through a solid-state single pore[1] provides a new method for biological analysis based on the size of targets, such as single-molecule detection,[2] discrimination,[3] DNA sequencing,[4−6] and cell analysis.[7] As demonstrated with α-hemolysin, bioanalysis with high selectivity and high sensitivity to target molecules can be achieved using biological-probe-modified nanopores.[8] A single pore with a biological-probe-functionalized inner wall can establish specific interactions with the targets, thus increasing the sensing selectivity.[9−11] A nanopore functionalized with a "probe" of hairpin loop DNA can selectively transport short "target" complementary single-stranded DNA with single-base mismatch sensitivity.[12] A protein biosensor based on a biofunctionalized conical gold nanopore embedded within a polymeric membrane has also been reported,[13] in which the protein analyte binds to a biochemical molecular-recognition agent immobilized at the small-diameter opening of the conical nanotube and provokes a corresponding permanent blockage of the ion current. Mimetic biological ion channels can be achieved using appropriately functionalized nanopores.[14−17]

However, the three-dimensional and tiny features of a single pore in a solid-state membrane make functionalization of its inner wall a challenge. Traditional surface modification methods have been employed for solid-state nanopore-wall modification to modulate the translocation behaviors of molecules, reduce detection noise, or establish a specific interaction with a desired target. Previous examples of nanopore functionalization include gold or alumina chemical deposition onto silicon nitride nanopore walls,[18,19] gold electroless plating onto a nanopore fabricated in a polymer membrane,[20,21] self-assembled monolayers using gold−thiol chemistry[13] or surface charges,[22] and silanization on the silica[12] or alumina[23] surface of nanopores. However, these methods offer low spatial selectivity because the surface of the inner wall is usually chemically similar to the bulk membrane. If a specific interaction between the grafted probe and the target is desired, the total functionalization of the pore wall and the bulk membrane would decrease the biosensing sensitivity because biological targets would be depleted by capture at the bulk membrane.

Many efforts have been made to locally functionalize the inner surface of single pores.[20−26] This objective can be achieved through the local chemical activation of the pore inner surface, followed by classic surface chemistry on this activated surface. The activation process represents a very complex step because of the identical chemical natures of the bulk membrane and the pore wall and the poor accessibility of the three-

Received: December 19, 2011
Accepted: February 24, 2012
Published: February 24, 2012

   dx.doi.org/10.1021/ac2033744 | Anal. Chem. 2012, 84, 3254−3261

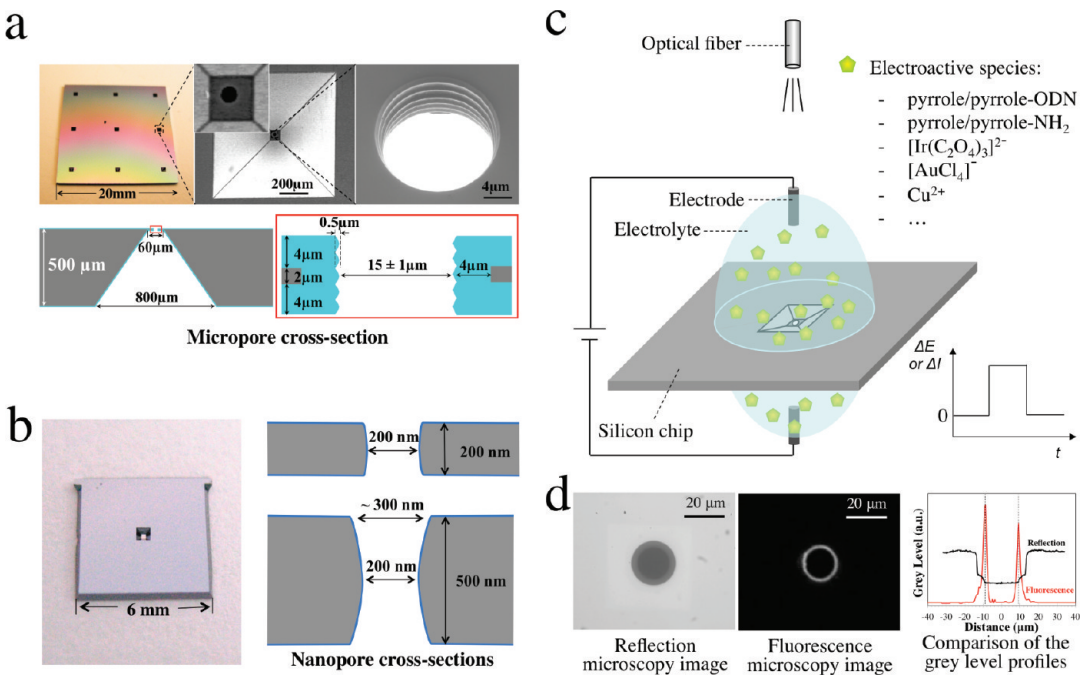

Figure 1. Pore chips and CLEF description. (a) Micropore chip and micropore cross-section diagram. (b) Nanopore chips and nanopore cross-section diagrams. (c) Schematic representation of single-pore functionalization using CLEF. (d) Reflection (left) and fluorescence (middle) microscopy characterizations of a micropore functionalized with PPy-ODN copolymers and hybridized with complementary biotinylated ODN coupled with streptavidin-*R*-phycoerythrin. Fluorescence intensity was measured along a line crossing the center of the ring and compared with the gray levels measured at the same place on the reflection microscopy image. The fluorescence acquisition conditions were as follows: acquisition time, 0.2 s; gain, ×1.

dimensional micro- to nanometer geometry of the pore wall. Ion-[24] or electron-[25] beam-assisted silica depositions have been used to locally modify the entrance of single nanopores fabricated in a silicon nitride membrane. Further functionalization of the nanopore with DNA probes was achieved through silane chemistry on the deposited silica.[24] A poly(ethylene terephtalate) (PET) membrane was irradiated by the ion-track technique and chemically etched with NaOH to create a conical channel in the membrane.[14,16,26,27] Concomitantly, carboxylic groups were created on the conical channel including the nanopore end as a result of the chemical etching process. These carboxylic groups allowed for the functionalization of the nanopore wall with desired molecules for biosensing. DNA chains can be immobilized on these carboxylic groups through a well-known peptidic coupling reaction.[15] In addition, the charge-transport properties of a conical nanopore in a PET membrane can be modulated through layer-by-layer polyelectrolyte assemblies on the channel inner wall surface.[28] Ionic diodes, in which an uneven surface charge is patterned on a conical nanopore, have been achieved for high-sensitivity biosensing.[29] Recently, a chiral sensing nanodevice based on a single conical nanochannel fabricated in a PET membrane and functionalized by chiral recognition elements was reported.[30] A one-step local modification of nanopores has also been realized by photoinduced polymerization of a monomer solution mechanically confined inside a porous membrane,[31] which generates gel-filled pores used for heavy-ion preconcentration. Recently, we reported a one-step method without mask patterning, called contactless electrofunctionalization (CLEF), that allows for the selective modification of the inner wall surface of a micropore either with polymers or metal oxide through electrochemical oxidation reactions[32] or with metals through electrochemical reduction reactions.[33]

Herein, according to a set of experimental and computation results, we demonstrate the CLEF mechanism and show the effect of the electric field amplitude and light excitation on the functionalization efficacy. Based on an understanding of the CLEF mechanism, nanopores were successfully functionalized by adjusting the amplitude of the applied electric field. A potential application of the functionalized nanopores for translocation-based bioanalysis is highlighted.

RESULTS AND DISCUSSION

CLEF for Micropore Functionalization. Micropores (15 μm in diameter) were etched in a silicon chip (Figure 1a), and a 4-μm-thick thermally grown silica layer covered the entire chip surface, including the micropore wall (Figure 1a, cross-sectional diagram). The principle of CLEF is illustrated in Figure 1c and described in section S1 of the Supporting Information. A micropore is placed within a homemade two-compartment holder (Supplementary Figure S1, Supporting Information). Both compartments are filled with an electrolytic solution containing electroactive species such as pyrrole/pyrrole-ODN, pyrrole/pyrrole-NH_2, $[Ir(C_2O_4)_3]^{2-}$, $[AuCl_4]^-$, or Cu^{2+} (Figure 1c). Upon application of a 2 V potential pulse between the electrodes immersed in each compartment, the micropore wall can be locally functionalized with copolymers, metal oxides, or metals. The current recorded as a function of time during the functionalization is illustrated in Supplementary Figure S2a (Supporting Information). It is worth noting that the pore silicon chip was not in direct contact with the electrodes, and no mask patterning of the membrane was used. Micropores functionalized with polypyrrole-ODN (PPy-ODN) copolymers can be characterized by fluorescence microscopy after biotinylation through hybridization and coupling with fluorescent-dye-labeled streptavidin (see the Supporting

dx.doi.org/10.1021/ac2033744 | *Anal. Chem.* 2012, 84, 3254−3261

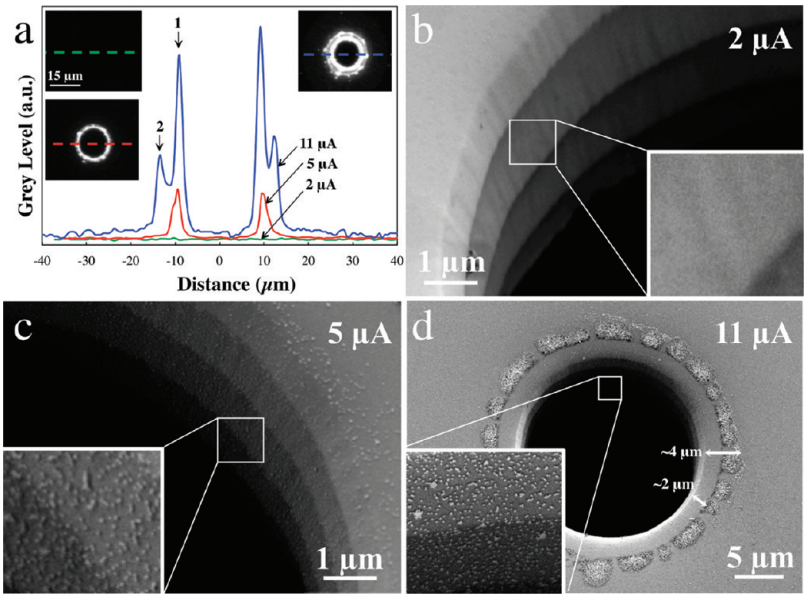

Figure 2. Role of the amplitude of the applied electric field. (a) Fluorescence characterization of micropores functionalized with PPy-ODN using current pulses of 2, 5, and 11 μA for 100 ms. Fluorescence intensities were measured along a line crossing the center of each micropore. Insets: Fluorescence microscopy images of the micropores. The fluorescence acquisition conditions for the micropore functionalized using 2 and 5 μA pulses were as follows: acquisition time, 0.2 s; gain, ×1. As the fluorescence of the micropore functionalized at 11 μA saturated the camera at an acquisition time of 0.2 s, another image was collected with an acquisition time of 0.04 s (gain ×1), and then the measured fluorescence intensities were multiplied by 5 for display in this figure. (b–d) SEM images of micropores functionalized with PPy-NH_2 copolymers using current pulses of (b) 2, (c) 5, and (d) 11 μA for 100 ms. Amine groups were used to trap 20-nm Au nanoparticles that served as contrast agents for SEM observation. The insets show Au nanoparticles deposited on the pore wall.

Information, section S1, for details). A fluorescent ring corresponding to the position of the pore wall (Figure 1d) demonstrates that the micropore wall is locally functionalized by PPy-ODN copolymers. SEM images of micropores illustrating electrodeposition of iridium oxide,[32] gold,[33] and copper[33] have been reported elsewhere.

The observed micropore-wall modification is a result of chemical reaction taking place inside the pore. Two hypotheses could explain the mechanism: (i) chemical reaction in the solution catalyzed by the high electric field (10^5 V/m)[32] in the micropore and (ii) electrochemical reaction occurring on the silica/electrolyte interface. According to the first hypothesis, nucleation and growth would take place in the bulk of the pore volume, with some of the generated oligomers or particles being further adsorbed onto the pore wall. This could explain the oxidation of pyrrole or iridium oxalate by dissolved oxygen residue. However, oxygen does not participate in metal reduction. Moreover, the electrolyte used for metal deposition in the micropore contains the following species: H_2O, H_2SO_4 and metal salts. These species cannot participate as reducing species in a homogeneous reaction within the pore volume. As a consequence, metal deposition invalidates the hypothesis dealing with the reaction of two species in the electrolyte accelerated by the high electric field inside the micropore. This result is reinforced by the PPy-ODN deposition in micropores in an inert atmosphere (Supporting Information, section S3). Therefore, the reactions more likely occur at the silica/electrolyte interface within the pore. The investigation of the mechanism was thus oriented toward understanding the effect of pore membrane polarization behavior on local pore-wall functionalization.

Effect of the Amplitude of the Applied Electric Field. Pore membrane polarization behavior is affected by the amplitude of the applied electric field. This amplitude was varied during the CLEF process to investigate its influence on PPy-ODN deposition. For this study, current pulses were applied instead of potential pulses to make the potential drop across the pore membrane independent of the electrode polarization behavior during functionalization. Three different current pulse intensities (2, 5, and 11 μA) were tested for micropore functionalization with PPy-ODN (Figure 2a). The recorded potentials as a function of time during the functionalization are illustrated in Supplementary Figure S2b (Supporting Information). No PPy-ODN is deposited at 2 μA, whereas localized deposition on the pore wall is obtained at 5 and 11 μA (Figure 2a). This suggests the existence of a threshold of electric field intensity in the pore above which the reaction occurs. At 11 μA, deposits were also observed on the membrane surface in the form of a discontinuous ring in the vicinity of the micropore (Figure 2a). This ring is concentric with the micropore, with a radius approximately 3 μm larger than that of the micropore.

A similar experiment was performed for polypyrrole-NH_2 (PPy-NH_2) copolymer deposition to precisely locate the deposited copolymers. Micropores functionalized with PPy-NH_2 were prepared using the three current pulse intensities: 2, 5, and 11 μA. Gold nanoparticles (20 nm) trapped by amine groups[34] were used as contrast agents for SEM characterization of the deposited layer (Figure 2b–d). At 2 μA, almost no Au nanoparticles were observed on the inner wall surface (Figure 2b). At 5 μA, a high density of nanoparticles was observed on the entire inner wall surface (Figure 2c). This result is in agreement with fluorescence observations of PPy-ODN-functionalized micropores (Figure 2a). In Figure 2c, an approximately 800-nm-wide contour around the micropore entry surface is covered with Au nanoparticles; 5 μA is thus a nearly optimal current intensity for local pore-wall functionalization in this micropore configuration. The 11-μA current

dx.doi.org/10.1021/ac2033744 | Anal. Chem. 2012, 84, 3254–3261

pulse functionalized the micropore wall as well as the vicinity of the membrane (Figure 2d). A layer of Au nanoparticles covers the micropore inner wall surface (Figure 2d, inset). Moreover, a discontinuous ribbon of nanoparticles is observed on the membrane in the vicinity of the micropore as a result of deposited copolymers. The nanoparticle ribbon is concentric with the micropore with an inner radius approximately 2 μm from the micropore edge and a width of approximately 2 μm. The position of this ring is in agreement with the second fluorescence peak at 11 μA depicted in Figure 2a.

The similar deposition patterns of PPy-ODN (Figure 2a) and of PPy-NH_2 (Figure 2c,d) are not a coincidence and highlight the impact of the applied electric field amplitude on CLEF functionalization efficiency and localization. There is an electric field intensity threshold above which reactions can take place. Moreover, under optimal electric field intensity, the reactions exclusively occur on the pore wall. With higher electric field intensity, a deposit was also observed on the membrane in the vicinity of the micropore.

Effect of the Electrical Properties of the Membrane. Membrane polarization behavior also depends strongly on the electrical properties of the membrane. To investigate the role of the electrical properties of the membrane in CLEF, the electrical conductivity of the silicon core of the membrane (Figure 1a) was modulated by controlling illumination levels, as light excitation can increase the electrical conductivity of silicon in an electric field.[35−37] Localized PPy-ODN deposition within the micropore was obtained when CLEF was performed under visible light illumination, and almost no deposition was observed when it was carried out in the dark (Figure 3).

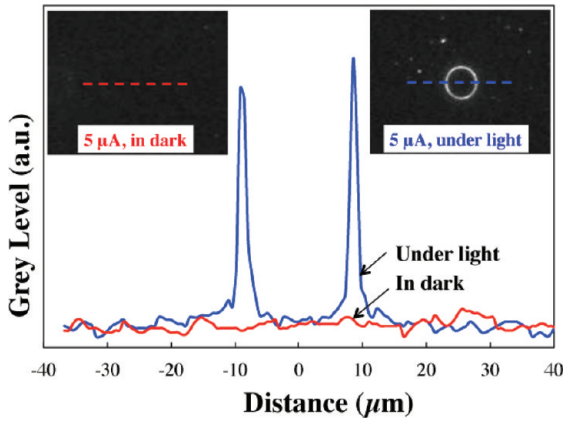

Figure 3. Effects of the membrane electrical properties. Fluorescence characterization of micropores after PPy-ODN deposition under light illumination or in the dark. Fluorescence intensities were measured along a line crossing the center of each micropore. Insets: Fluorescence microscopy images of the micropores. The fluorescence acquisition conditions for the two images were as follows: acquisition time, 0.2 s; gain, ×4.

Furthermore, no copolymer deposition was observed when a single pore etched in a Si_3N_4 membrane is used (data not shown). These results reveal the influence of the electrical properties of the pore membrane on pore-wall functionalization efficiency, and thus confirm the pore membrane polarization hypothesis.[33] The fact that silicon core conductivity influences functionalization efficiency on the pore wall suggests there is a radial electrical pathway between the pore-wall surface and the silicon core of the membrane.

Numerical Modeling of the Electric Field near the Micropore. To investigate the membrane polarization behavior, we studied the electric field distribution and orientation near the micropore using numerical modeling. Numerical simulations were performed using the finite-element code Comsol Multiphysics. To verify whether the mathematical model used in the numerical simulations adequately represents the electric behavior of the micropore membrane, we compared the measured and simulated impedance (Z) norm and phase curves as a function of the applied potential frequency (Figure 4a). Despite a frequency shift between the theoretical curve and experimental data, the shape of the simulated curves is in agreement with the measured curves, which validates the simulation model. The difference in frequency might result from the fact that the model is simplistic; some important physical parameters, such as the electrical behavior of the silica/silicon and silica/electrolyte interfaces, light illumination, and other factors, are not taken into account. The computation of the electric field distribution might therefore be instructive for the micropore membrane polarization behavior.

The electric field norm with current density vectors within the micropore and in the micropore vicinity, under an applied potential of 2 V, is shown in Figure 4b. As a result of the geometric restriction of the micropore, the electric field intensity inside the pore is as high as 10^5 V/m. The electric field intensity strongly decreases outside the micropore, to approximately 20−30 V/m in the bulk electrolyte. This result clearly shows the confinement of the electric field inside the micropore, which can also be observed from the distribution in magnitude of the current density vectors (Figure 4b). The electric field in the silicon dioxide layer of the bulk membrane is as high as $\sim 2 \times 10^5$ V/m because of its low electrical conductivity (Figure 4b) and exclusively composed of the axial electric field (comparison between Figure 4b and 4c). In the silicon dioxide layer that composes the inner wall of the micropore, the electric field norm is heterogeneous and lower than that of the silica layer composing the bulk membrane (Figure 4b). The radial component of the electric field (E_r) near the micropore is shown in Figure 4c. The E_r intensity is maximal at the edges of the pore with a value of approximately $\pm 10^5$ V/m and is about $\pm 3 \times 10^4$ V/m along the pore surface until the pore edges (Figure 4c). Conversely, E_r is negligible in the bulk electrolyte, in the silicon dioxide layer of the bulk membrane, and in the silicon layer. In addition, the radial electric field directions are affected by the topology of the pore wall and present several reversals as a result of the scalloped micropore wall. The radial electric field in the silicon dioxide layer of the pore wall might be a result of (i) the confinement of the electric field caused by the geometric restriction of the micropore, which changes the electric field direction, as seen in the current vectors in Figure 4b, or (ii) the asymmetric geometry on each side of this silica layer: one side is the electrolyte, and the other side is the silicon core. As an electrical pathway between the micropore wall and the silicon core has been approved (Figure 3), we can now confirm that the radial electric field E_r is the driving force for the electrochemical reactions taking place on the inner wall surface of the micropore,[33] and the reversals of E_r along the pore wall can explain why both electro-oxidation (pyrrole polymerization) and electro-reduction (metal salt reduction) reactions occur in the micropore using the same protocol.

Defects in the Silica Layer. Despite the high axial electric field intensity in the silica layer on the bulk membrane (Figure

dx.doi.org/10.1021/ac2033744 | Anal. Chem. 2012, 84, 3254−3261

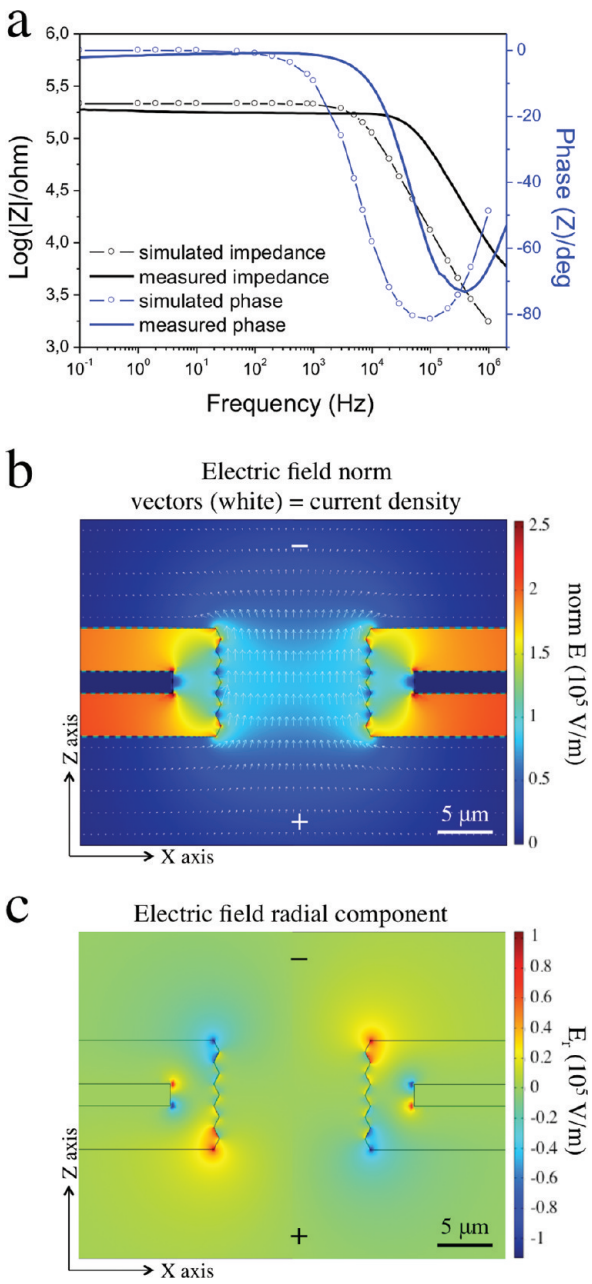

Figure 4. Numerical modeling of a micropore in an electrical field. (a) Comparison of the simulated and measured impedance spectra of a micropore in an electric field as a function of the applied potential frequency. (b) Electric field norm (colors) with current density vectors (white arrows) in the vicinity of the micropore at an applied voltage of 2 V (peak-to-peak intensity of the applied sinusoid signal). (c) Electric-field radial component (E_r), which represents the electric field in the direction perpendicular to the pore axis. Positive and negative field values indicate a radial electric field E_r pointing to the right and to the left, respectively. Although calculations were performed considering the two-dimensional axial symmetry of the electrolytic cell, the results are displayed here using a three-dimensional slice representation for ease of interpretation.

4b), almost no electrodeposition occurs on the membrane under optimal conditions (Figure 2c). We thus believe that the nature of the pore-wall silica layer differs from that of the bulk membrane. The silica layer was grown by the thermal oxidation of a silicon membrane containing a micropore of approximately 19 μm in diameter. After oxidation, a silica layer of approximately 4-μm thickness was formed, and the diameter of the micropore shrank to approximately 15 μm as a result of the swelling of the membrane during oxidation (Figure 1a). Usually, the 4-μm-thick silica that covers the chip surface and the pore wall is considered as an insulating layer.[38] However, pore diameter shrinkage as a result of thermal oxidation exerts a strong mechanical stress near the micropore,[39,40] which might provoke defects or fissures in the silica layer.[41]

We observed from a top-view SEM image that the micropore is not a perfect ring (Figure S6a) and should have been deformed by the mechanical stress in the silica layer. After HF treatment of the chip at 80 °C for 1 h to remove the silica layer, the remaining silicon micropore of approximately 23 μm in diameter appears to be an almost perfect ring (Figure S6b). As the mechanical stress is mainly exerted near the micropore, we believe that the silica layer in this area contains more defects than the bulk membrane. Moreover, the high silica thickness (4 μm) and scalloped inner wall surface might also promote defect formation in the layer. These defects in the silica layer near the micropore might increase the local electrical conductivity,[42−45] which could explain the electrical pathway between the pore-wall surface and the silicon core in the membrane. On the contrary, the silica layer on the bulk membrane surface contains fewer defects and can be considered as a dielectric layer, as no electrodeposition occurs on the membrane. The distribution of defects strongly depends on the geometry of the silicon before oxidation; it can explain the cyclic deposition in the vicinity of the micropore (Figure 2c). In addition, deposits were also observed on the other side of a membrane with a pyramidal opening (Figure 1a, inset SEM image) under 11 μA. Instead of cyclic, the form of deposits on this side is irregular. We believe that the distribution of defects in the membrane on this side is affected by both the cyclic micropore and the square bottom of the pyramidal opening.

Mechanism Proposal. The main components of the CLEF mechanism emerge from the experimental and simulation results obtained so far using the micropore. During CLEF, the silica layer of the micropore membrane insulates the bulk membrane surface and confines the electric field to the micropore. The electric field confinement and the sandwich-like membrane structure induce a radial electric field in the pore-wall silica layer that is proportional to the applied electric field intensity (Figure 2). In addition, the defects in the pore-wall silica layer enable an electrical pathway between the pore-wall surface and the silicon core. Under an adapted external electric field, electroactive species in the electrolyte can exchange electrons with the pore-wall surface, and electrodeposition occurs locally on the pore wall as a result of the silica layer defects. As several reversals of the radial electric field exist on the scalloped micropore wall (Figure 4c), both electro-oxidation and electro-reduction can take place on the pore wall depending on the electroactive species used. Because no relationship between the reaction time and the quantity of deposited matter was observed,[32,33] we assume that the pore-wall silica layer does not behave as a "classical" electrode; current might not continuously travel through defects in the silica layer during functionalization. It is more likely that the reactions are caused by the discharge of the capacitor formed at the electrolyte/silica and silica/silicon interfaces through defects in the silica layer.

According to this proposed mechanism, we can thus list the two essential factors to have localized electrodeposition in a single pore. First, a sandwich-like pore membrane structure

dx.doi.org/10.1021/ac2033744 | Anal. Chem. 2012, 84, 3254−3261

with a semiconducting or conducting core layer covered by an insulating layer is required. When the membrane has a semiconducting core layer, light illumination during deposition might be necessary to increase the charge-carrier density in the membrane (Figure 3). This property can be used as a controlling method for selective modification of a single pore by illuminating one pore in an array. Second, the electric field across the single pore can be optimized to obtain deposition only on the pore wall, as illustrated in Figure 2. For PPy-ODN deposition in the 15-μm micropore, the optimal current pulse intensity is 5 μA, corresponding to a current density of 2.8 A/cm^2 inside the micropore. We think that this optimal current density is determined by both the electrical properties of the pore membrane and the ionic concentration of the electrolyte.

According to the CLEF mechanism, the pore diameter and depth should not be limiting factors for the CLEF phenomenon, especially for smaller pore diameters, such as submicrometer- and nanometer-range pores, or longer channels made in a substrate. On the contrary, as localized electrodeposition is a result of the electric pathway between the silicon core and the pore-wall surface through local defects in the silica layer, the silica layer thickness might have an impact on the localized electrodeposition. As shown above, a silica layer thickness up to 4 μm allowed for localized pore-wall functionalization. We will investigate in the following section whether a native silica layer also allows the local pore-wall modification. For this purpose, the functionalization of a nanopore etched in a silicon membrane and covered by a native silica layer was assayed using CLEF.

Nanopore Functionalization Using CLEF. The capacity of CLEF to locally functionalize nanopore walls was investigated using 200-nm nanopores etched in a silicon membrane and covered with a native oxide layer (Figure 1b). As shown above, the adapted current density used to functionalize a 15-μm-wide micropore was 2.8 A/cm^2 inside the pore (Figure 2c). A similar current density was applied to functionalize the nanopore in this experiment, in which the pore diameter was assumed to be the main parameter determining the necessary current intensity for localized functionalization. A current pulse of 1 nA (3.2 A/cm^2 inside the nanopore) was thus applied for 100 ms to obtain a PPy-NH_2-functionalized nanopore. In a control experiment, the sample was immersed in the electrolyte, but no current pulse was applied. After incubation with 20-nm Au colloids, the samples were characterized by SEM (Figure 5). A high density of adsorbed Au nanoparticles was observed on the pore wall of the functionalized sample (Figure 5a) as compared to the control sample (Figure 5b). This higher nanoparticle density is the result of the deposited PPy-NH_2 copolymers. This result confirms that CLEF can also be used for nanopore functionalization.

The density of Au nanoparticles on the membrane in the vicinity of the functionalized nanopore is slightly higher than that of the nonfunctionalized one (Figure 5a,b), which suggests that a few PPy-NH_2 molecules might also be deposited in this area. In addition, few nanoparticles were observed on the bulk membranes of the functionalized and control samples, which might be a result of nonspecific adsorption. The limited deposition on the bulk membrane indicates that the native silica layer efficiently insulates the bulk membrane during the functionalization. We think that the deposits in the vicinity of the functionalized nanopore are also a result of defects in this area due to the thinning process of the membrane. The above

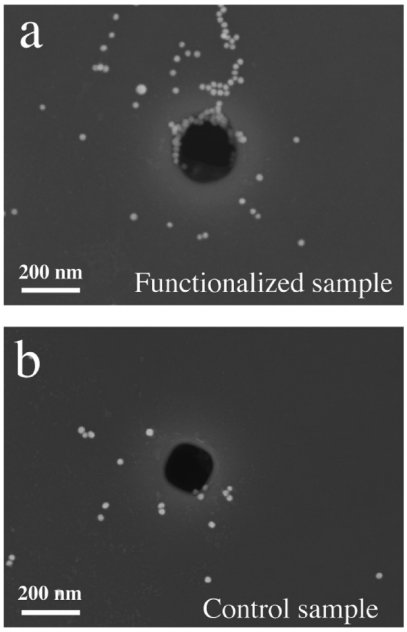

Figure 5. Nanopore functionalization using CLEF. (a) SEM image of a 200-nm nanopore after PPy-NH_2 deposition using CLEF and incubation with 20-nm Au colloids. A high density of Au nanoparticles in the nanopore can be observed on the nanopore wall. Some particles are also present on the silicon membrane in the vicinity of the nanopore. (b) Similar nanopore after being immersed in the deposition solution without application of the current pulse and then incubated with the Au colloids, as a control. Fewer nanoparticles can be observed in the nanopore and in the membrane.

results confirm the proposed CLEF mechanism and show that the pore diameter is not a limiting factor for the CLEF phenomenon.

Biosensing Using a CLEF-Functionalized Single Pore. The efficacy of nanopore functionalization using CLEF motivated an investigation of translocation-based biosensing through specific biological interactions. The principle of detection is illustrated in Figure 6a. A 200-nm nanopore was functionalized with PPy-ODN copolymers and treated with bovine serum albumin (BSA) to prevent nonspecific adsorption onto the membrane surface. Au nanoparticles (100 nm in diameter) were coated with complementary ODN or non-complementary ODN (hereafter referred to as c-ODN-AuNP and nc-ODN-AuNP, respectively). These negatively charged nanoparticles were driven to and translocated through the functionalized nanopore by a stationary electric field. A specific target can be slowed or captured by the pore-wall copolymers, whereas a nonspecific target should pass through without any specific interaction.

The translocation experiments on both c-ODN-AuNP and nc-ODN-AuNP were performed sequentially using the same functionalized nanopore with an injection system (Supplementary Figure S5, Supporting Information). Typical current versus time traces obtained for nc-ODN-AuNPs display steady and nonblockaded translocations[46,47] of these nanoparticles through the nanopore under a bias potential of 500 mV (Figure 6b). The baseline current intensity (I_0) of this curve was about 180 nA. This relatively high bias potential was chosen because, under lower bias potential (400 mV), the translocation-induced variation in current amplitude was too low (about 0.08 nA) and barely distinguishable from the baseline noise (Supplementary

dx.doi.org/10.1021/ac2033744 | Anal. Chem. 2012, 84, 3254−3261

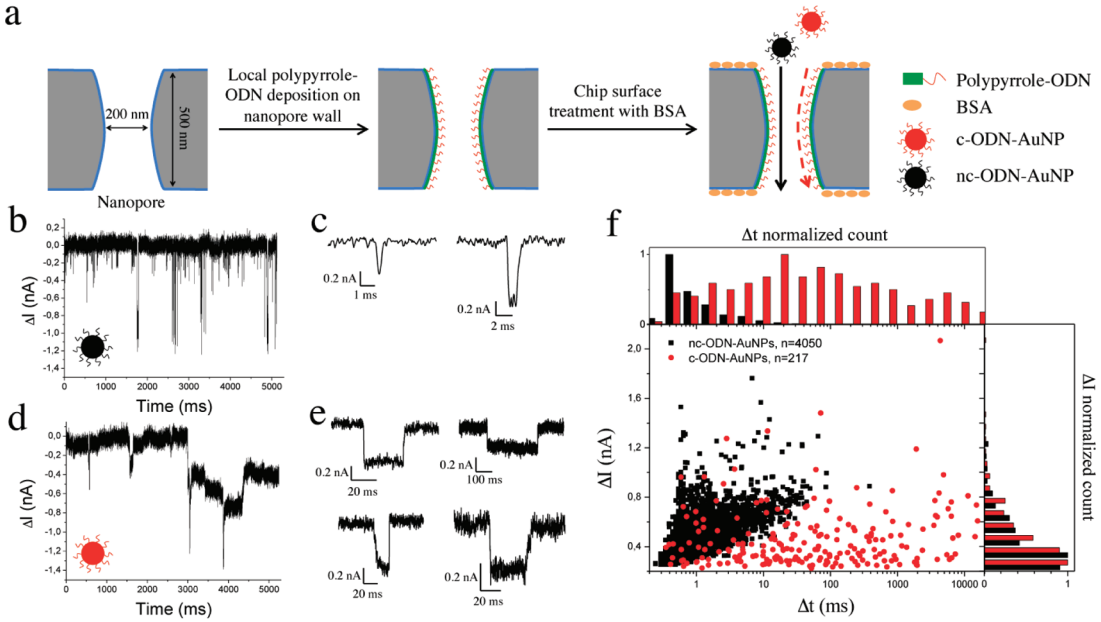

Figure 6. Biosensing with a functionalized nanopore. (a) Schematic illustration of the biosensing principle. (b–f) Translocation of nanoparticles (100 nm in diameter) through a PPy-ODN-functionalized nanopore (200 nm in diameter). (b) Example of a current versus time trace for the translocation of nc-ODN-AuNPs through the functionalized nanopore. (c) Two typical events corresponding to the translocation of a single nanoparticle (left) and a small nanoparticle aggregate (right). (d) Example of a current versus time trace for the translocation of c-ODN-AuNPs through the same nanopore. (e) Several current trace examples illustrating the extended blockade times of c-ODN-AuNPs within the functionalized nanopore. (f) Scatter plots of the change in current amplitude (ΔI) versus the duration (Δt) of translocation events and distributions of ΔI and Δt.

Figure S7, Supporting Information), as a result of the high current noise of the silicon membrane.[48,49] Translocation events with current variations of different amplitudes (ΔI) were observed (Figure 6c). This might be a result of the translocation of either a single nanoparticle or small aggregates of nanoparticles (Supplementary Figure S4, Supporting Information). The current traces of c-ODN-AuNPs showed different characteristics (Figure 6d); extended translocation times were observed for complementary nanoparticles (Figure 6e) as compared to noncomplementary nanoparticles (Figure 6b,c). Moreover, when ODN-modified nanopores with greater diameter (500 nm) were used, the translocation of c-ODN-AuNPs showed permanent blockage of the nanopore (Supplementary Figure S8, Supporting Information).

The scatter plots of current variation amplitude versus translocation time and the associated ΔI and Δt distributions for both c-ODN-AuNPs and nc-ODN-AuNPs are shown in Figure 6f. The ΔI distributions of the two types of nanoparticles show comparable profiles. This result suggests that the diameter distributions of nanoparticles and their aggregation states are similar in the two samples. The average ΔI values for the two types of nanoparticles are similar, about 0.47 nA. In general, the ratio of ΔI to the baseline current intensity is roughly the same as the nanoparticle volume relative to the channel volume.[50,51] However, in our case, the $\Delta I/I_0$ value was obviously lower than the ratio of the nanoparticle volume to the nanopore volume as a result of the high capacitance of the membrane,[51] which is composed of *n*-type doped silicon (resistivity of 0.010–0.025 Ω·cm) and covered by a native silica layer. The Δt distributions of the two types of nanoparticles were significantly different (Figure 6f): the translocation times of c-ODN-AuNPs varied from 0.3 ms to 20 s (average, 490 ms), whereas the translocation times for nc-ODN-AuNPs were mainly in the range of 0.3 to 50 ms (average, 2.2 ms). The longer Δt for complementary nanoparticles is undoubtedly caused by specific interactions between ODNs on the pore wall and the nanoparticle surfaces. Furthermore, most nc-ODN-AuNP translocations were short (from 0.3 to 2 ms), whereas c-ODN-AuNP translocations had significant occurrences from 0.3 ms to 10 s. The wide range of translocation times for c-ODN-AuNPs very likely arises from both a variable number of specific interactions established between the nanoparticle and the pore wall and a distribution of nanoparticle velocities within the pore (revealed by the Δt distribution for nc-ODN-AuNP translocations).

These results clearly demonstrate the capability of functionalized nanopores to discriminate between nanoparticles through specific biological interactions. Nonoptimal nanopore diameter and depth were used in this proof-of-concept experiment. The pore diameter (200 nm in the pore central region) and depth (500 nm) were 2 and 5 times larger, respectively, than the nanoparticle diameter. This might be the main reason for the variable translocation times of the specific target c-ODN-AuNPs. Other experimental conditions such as temperature, ion concentration, or electric bias voltage might also play an important role in the translocation behavior of targets[52] and will have to be optimized for the analysis of future biological targets.

■ CONCLUSIONS

Membrane-polarization-induced local pore-wall functionalization is described in this article. CLEF is a versatile method: both electro-oxidation and electro-reduction chemistries can be used for pore functionalization, and pore size can range from micrometric to nanometric. Two factors are essential for local functionalization: (i) a sandwich-like pore membrane structure with a conducting or semiconducting core and a dielectric cover layer and (ii) an optimized potential difference across the pore membrane, which depends on pore diameter and membrane

dx.doi.org/10.1021/ac2033744 | *Anal. Chem.* 2012, 84, 3254–3261

electrical properties. This reliable one-step method locally functionalizes single pores with the desired (bio)molecules, an essential requirement for nanopore-based biosensing and biomimetic ionic channels.[53] Furthermore, as the surface to be functionalized is not in direct contact with the electrodes, CLEF can be used to functionalize surfaces, such as the inside of tridimensional mechanical structures or microfluidic channels, that are inaccessible using conventional methods.

■ ASSOCIATED CONTENT

Supporting Information

Experimental section and additional experimental data as noted in the text. This material is available free of charge via the Internet at http://pubs.acs.org.

■ AUTHOR INFORMATION

Corresponding Author

*Tel.: +33 4 38 78 35 36 (J.L.), +33 4 79 60 15 35 (P.M.). Fax: +33 4 38 78 51 45 (J.L.), +33 4 79 68 80 49 (P.M.). E-mail: jie.liu1@cea.fr (J.L.), pascal.mailley@cea.fr (P.M.).

Notes

The authors declare no competing financial interest.

■ ACKNOWLEDGMENTS

This work was financially supported by the ANR agency under the PNANO program (Grant PRECIS ANR-08-NANO-049-02). We thank R. Calemczuk, Y. Roupioz, X. Gidrol, A. Tixier-Mita, and J.-C. Barbé for fruitful discussions; M. De Waard, N. Picollet-D'hahan, L. Ghenim-Ziman, and A. Boussaoud for their help in the experiments; and C. Pudda for chip fabrication.

■ REFERENCES

(1) Dekker, C. *Nat. Nanotechnol.* **2007**, *2*, 209−215.
(2) Mara, A.; Siwy, Z.; Trautmann, C.; Wan, J.; Kamme, F. *Nano Lett.* **2004**, *4*, 497−501.
(3) Skinner, G. M.; van den Hout, M.; Broekmans, O.; Dekker, C.; Dekker, N. H. *Nano Lett.* **2009**, *9*, 2953−2960.
(4) Sigalov, G.; Comer, J.; Timp, G.; Aksimentiev, A. *Nano Lett.* **2008**, *8*, 56−63.
(5) Luan, B.; Peng, H.; Polonsky, S.; Rossnagel, s.; Stolovitzky, G.; Martyna, G. *Phys. Rev. Lett.* **2010**, *104*, 4.
(6) Timp, W.; Mirsaidov, U. M.; Wang, D.; Comer, J. *IEEE Trans. Nanotechnol.* **2010**, *9*, 281−294.
(7) Ogura, E.; Abatti, P. J.; Moriizumi, T. *IEEE Trans. Bio-med. Electron.* **1991**, *38*, 721−726.
(8) Bayley, H.; Cremer, P. S. *Nature* **2001**, *413*, 226−230.
(9) Howorka, S.; Siwy, Z. *Chem. Soc. Rev.* **2009**, *38*, 2360−2384.
(10) Gyurcsányi, R. E. *Trends Anal. Chem.* **2008**, *27*, 627−639.
(11) Sexton, L. T.; Horne, L. P.; Martin, C. R. *Mol. BioSyst.* **2007**, *3*, 667−685.
(12) Iqbal, S. M.; Akin, D.; Bashir, R. *Nat. Nanotechnol.* **2007**, *2*, 243−248.
(13) Siwy, Z.; Trofin, L.; Kohli, P.; Baker, L. A.; Trautmann, C.; Martin, C. R. *J. Am. Chem. Soc.* **2005**, *127*, 5000−5001.
(14) Xia, F.; Guo, W.; Mao, Y.; Hou, X.; Xue, J.; Xia, H.; Wang, L.; Song, Y.; Ji, H.; Ouyang, Q.; Wang, Y.; Jiang, L. *J. Am. Chem. Soc.* **2008**, *130*, 8345−8350.
(15) Yameen, B.; Ali, M.; Neumann, R.; Ensinger, W.; Knoll, W.; Azzaroni, O. *Nano Lett.* **2009**, *9*, 2788−2793.
(16) Hou, X.; Guo, W.; Xia, F.; Nie, F.-Q.; Dong, H.; Tian, Y.; Wen, L.; Wang, L.; Cao, L.; Yang, Y.; Xue, J.; Song, Y.; Wang, Y.; Liu, D.; Jiang, L. *J. Am. Chem. Soc.* **2009**, *131*, 7800−7805.
(17) Calvo, A.; Yameen, B.; Williams, F. J.; Soler-Illia, G. J. A. A.; Azzaroni, O. *J. Am. Chem. Soc.* **2009**, *131*, 10866−10868.
(18) Chen, P.; Mitsui, T.; Farmer, D. B.; Golovchenko, J.; Gordon, R. G.; Branton, D. *Nano Lett.* **2004**, *4*, 1333−1337.
(19) Wei, R.; Pedone, D.; Zurner, A.; Doblinger, M.; Rant, U. *Small* **2010**, *6*, 1406−1414.
(20) Martin, C. R.; Nishizawa, M.; Jirage, K.; Kang, M. *J. Phys. Chem. B* **2001**, *105*, 1925−1934.
(21) Siwy, Z.; Heins, E.; Harrell, C. C.; Kohli, P.; Martin, C. R. *J. Am. Chem. Soc.* **2004**, *126*, 10850−10851.
(22) Wanunu, M.; Meller, A. *Nano Lett.* **2007**, *7*, 1580−1585.
(23) Kim, Y.-R.; Min, J.; Lee, I.-H.; Kim, S.; Kim, A.-G.; Kim, K.; Namkoong, K.; Ko, C. *Biosens. Bioelectron.* **2007**, *22*, 2926−2931.
(24) Nilsson, J.; Lee, J. R. I.; Ratto, T. V.; Létant, S. E. *Adv. Mater.* **2006**, *18*, 427−431.
(25) Danelon, C.; Santschi, C.; Brugger, J.; Vogel, H. *Langmuir* **2006**, *22*, 10711−10715.
(26) Xu, H.; Hua, D.; Daoben, Z.; Lei, J. *Small* **2010**, *6*, 361−365.
(27) Ali, M.; Yameen, B.; Neumann, R.; Ensinger, W.; Knoll, W.; Azzaroni, O. *J. Am. Chem. Soc.* **2008**, *130*, 16351−16357.
(28) Ali, M.; Yameen, B.; Cervera, J.; Ramirez, P.; Neumann, R.; Ensinger, W.; Knoll, W.; Azzaroni, O. *J. Am. Chem. Soc.* **2010**, *132*, 8338−8348.
(29) Vlassiouk, I.; Kozel, T. R.; Siwy, Z. S. *J. Am. Chem. Soc.* **2009**, *131*, 8211−8220.
(30) Han, C.; Hou, X.; Zhang, H.; Guo, W.; Li, H.; Jiang, L. *J. Am. Chem. Soc.* **2011**, *133*, 7644−7647.
(31) Vasudevan, T.; Das, S.; Sodaye, S.; Pandey, A. K.; Reddy, A. V. R. *Talanta* **2009**, *78*, 171−177.
(32) Bouchet, A.; Descamps, E.; Mailley, P.; Livache, T.; Chatelain, F.; Haguet, V. *Small* **2009**, *5*, 2297−2303.
(33) Liu, J.; Hébert, C.; Pham, P.; Haguet, V.; Mailley, P.; Livache, T. *Small*, published online Mar 2, 2012, http://dx.doi.org/10.1002/smll.201102327.
(34) Mukhopadhyay, K.; Phadtare, S.; V.P., V.; Kumar, A.; Rao, M.; Chaudhari, R. V.; Sastry, M. *Langmuir* **2003**, *19*, 3858−3863.
(35) Fujii, H.; Kanemaru, S.; Matsukawa, T.; Hiroshima, H.; Yokoyama, H.; Itoh, J. *Jpn. J. Appl. Phys.* **1998**, *37*, 7182−7185.
(36) Francinelli, A.; Tonneau, D.; Clement, N.; Abed, H.; Jandard, F.; Nitsche, S.; Dallaporta, H.; Safarov, V.; Gautier, J. *Appl. Phys. Lett.* **2004**, *85*, 5272−5274.
(37) Burgelman, M.; Minnaert, B. *Thin Solid Films* **2006**, *511−512*, 214−218.
(38) Picollet-D'hahan, N.; Sordel, T.; Garnier-Raveaud, S.; Sauter, F.; Ricoul, F.; Pudda, C.; Marcel, F.; Chatelain, F. *Sensor Lett.* **2004**, *2*, 91−94.
(39) Kao, D. B.; Saraswat, K. C.; McVittie, J. P.; Nix, W. D. *IEEE Trans. Electron Devices* **1985**, *32*, 2530−2531.
(40) Szekeres, A.; Danesh, P. *Semicond. Sci. Technol.* **1996**, *11*, 1225−1230.
(41) Liang, Y.; Miranda, C. R.; Scandolo, S. *Phys. Rev. B* **2007**, *75*, 024205.
(42) DiMaria, D. J.; Cartier, E. *J. Appl. Phys.* **1995**, *78*, 3883−3894.
(43) Blochl, P. E.; Stathis, J. H. *Phys. Rev. Lett.* **1999**, *83*, 372.
(44) Blochl, P. E. *Phys. Rev. B* **2000**, *62*, 6158−6179.
(45) Huang, J. Q.; Huang, Q. A.; Qin, M.; Dong, W.; Chen, X. *J. Microelectromech. Syst.* **2010**, *19*, 1521−1523.
(46) Prabhu, A. S.; Jubery, T. Z. N.; Freedman, K. J.; Mulero, R.; Dutta, P.; Kim, M. J. *J. Phys.: Condens. Matter* **2010**, *22*, 454107.
(47) Astier, Y.; Datas, L.; Carney, R.; Stellacci, F.; Gentile, F.; DiFabrizio, E. *Small* **2011**, *7*, 455−459.
(48) Tabard-Cossa, V.; Trivedi, D.; Wiggin, M.; Jetha, N. N.; Marziali, A. *Nanotechnology* **2007**, *18*, 305505.
(49) Uram, J. D.; Ke, K.; Mayer, M. *ACS Nano* **2008**, *2*, 857−872.
(50) DeBlois, R. W.; Bean, C. P. *Rev. Sci. Instrum.* **1970**, *41*, 909−916.
(51) Ito, T.; Sun, L.; Henriquez, R. R.; Crooks, R. M. *Acc. Chem. Res.* **2004**, *37*, 937−945.
(52) Fologea, D.; Uplinger, J.; Thomas, B.; McNabb, D. S.; Li, J. *Nano Lett.* **2005**, *5*, 1734−1737.
(53) Yusko, E. C.; Johnson, J. M.; Majd, S.; Prangkio, P.; Rollings, R. C.; Li, J.; Yang, J.; Mayer, M. *Nat. Nanotechnol.* **2011**, *6*, 253−260.